Journal of Organometallic Chemistry 695 (2010) 963–969

Contents lists available at ScienceDirect

Journal of Organometallic Chemistry

journal homepage: www.elsevier.com/locate/jorganchem

Structural elucidation of transition metal complex by single crystal EPR study

S. Boobalan, P. Sambasiva Rao *

Department of Chemistry, Pondicherry University, Puducherry 605 014, India

ARTICLE INFO

Article history:
Received 23 September 2009
Received in revised form 22 January 2010
Accepted 22 January 2010
Available online 1 February 2010

Keywords:
Spin-Hamiltonian
Crystal field
Hyperfine coupling
Percentage covalency
Bonding parameters

ABSTRACT

Single crystal EPR studies of Mn(II) doped hexaaquazincdiaquabis(malonato) zincate $[Zn(H_2O)_6]$-$[Zn(mal)_2(H_2O)_2]$ have been carried out at room temperature using X-band spectrometer to identify the location of the dopant. Single crystal rotations along the three orthogonal axes show more than 30 line pattern EPR spectra indicating the presence of two types of dopant ions in the host lattice, with intensity ratio of 6:1. However, the latter could not be followed due to its low intensity during crystal rotations. The spin-Hamiltonian parameters, estimated from the three mutually orthogonal crystal rotations are: $g_{xx} = 1.972$, $g_{yy} = 2.000$, $g_{zz} = 2.023$, $A_{xx} = 8.95$, $A_{yy} = 9.48$, $A_{zz} = 9.93$ mT, $D_{xx} = -34.49$, $D_{yy} = -3.26$, $D_{zz} = 37.74$ mT and $E = 15.6$ mT. The direction cosines of one of the principal values of g match with that of Zn–O bond in the host lattice, suggesting that the Mn(II) ion entered the lattice substitutionally. The large value of E is indicative of low symmetry of the substitutional site, in accordance with the crystal structure of the isomorphous $[Zn(H_2O)_6][Cu(mal)_2(H_2O)_2]$. Covalency of Mn–O bond, estimated from Matamura's plot, is 9%. Various admixture coefficients, bonding and optical parameters have also been calculated.

1. Introduction

Out of all the first row transition metal ions, EPR studies of Mn(II), high spin d^5 ion, plays an important role, as it has five 3d electrons and the ground state is $^6S_{5/2}$. As the resultant angular momentum is zero, only the electron spin is responsible for the paramagnetism. If the ground state is a pure sextet, then the EPR spectrum would be a single line at free-spin value of 2.0023, because all the five $\Delta M_S = \pm 1$ transitions have the same energy. In addition, the S-state ions are characterized by long spin lattice relaxation times; it gives well resolved EPR spectra even at room temperature [1,2]. Hence, these ions have been studied in a variety of crystal lattices [3–5] by EPR technique. Moreover, the zero-field splitting is very sensitive even to minute distortions [6] and hence gives explicit information about the crystal symmetry and phase transitions of the host lattice [7–10]. The main emphasis of the EPR studies of Mn(II) in crystals has been the determination of site symmetries and orientations, the study of phase transitions and the magnetic properties of the host lattices. In addition, the effect of charge compensation is also studied in Mn(II) doped single crystals. The impurity ions, such as transition metal ions, are responsible for modification of many physical properties and play a major role in devices like wave-guides, holography and electro-optical devices [11]. Mn(II) ion has been used as a probe in large varieties of host lattices because it shows no Jahn–Teller effect and hence its EPR spectra reflect the true point symmetry.

EPR study of Mn(II) in different host lattices indicate that it can enter the lattice either substitutionally/interstitially or both [12,13]. Malonic acid also acts as a ligand with various dentate abilities. Coordination polymer compounds containing malonic acid as a ligand have been studied due to their potential application as materials in molecular electronics, catalysts, biologically active compounds, molecular-based magnetic materials, microporosity, electrical conductivity, non-linear optical activity, etc. [14,15]. Coordination compounds containing malonic acid as a ligand have potential application as materials in molecular electronics, catalysts, biologically active compounds, molecular-based magnetic materials, etc. [14,15]. Additionally, the carboxylate group provides an efficient pathway that couples the magnetic centres either ferro- or antiferromagnetically [16–22], the coupling constant being influenced by structural aspects such as the conformation of the bridge or the geometry of the metal environment. Organic complexes of manganese(II) have studied due to their magnetic interactions [23,24], formation of self-assemblies of molecular rods and tubes where long distance phenomena, such as the electron-energy transfer or magnetic coupling in transition ions, which can be changed by structural modifications [25,26] and in view of short or long order magnetic states [23,24].

Hence the present study of Mn(II) in hexaaquazincdiaquabismalonato zincate (hereafter abbreviated as HZBMZ) was carried out to ascertain site symmetry, location and also to predict the extent

* Corresponding author. Address: Department of Chemistry, Pondicherry University, R.V. Nagar, Kalapet, Puducherry 605 014, India. Tel.: +91 413 2654412; fax: +91 413 2655987.
E-mail address: psr52in@yahoo.co.in (P.S. Rao).

0022-328X/$ - see front matter © 2010 Elsevier B.V. All rights reserved.
doi:10.1016/j.jorganchem.2010.01.028

of distortion. Also, the relative signs of the zero-field parameters have been ascertained and the percentage covalency of the metal–ligand has been estimated.

2. Experimental

2.1. Materials and methods

Malonic acid, basic zinc(II) carbonate and zinc acetate were purchased from commercial sources and used as received. The EPR studies were performed on a JEOL JES-TE100 ESR spectrometer operating at X-band frequencies, having a 100 kHz field modulation to obtain the first-derivative EPR spectrum at room temperature. 1,1-Diphenyl-2-picrylhydrazyl (DPPH) with a *g*-value of 2.0036 is used as a reference for *g*-factor calculations. FT-IR spectra of doped and undoped materials in the frequency range of 4000–400 cm^{-1} were recorded on a Shimadzu FT-IR-8300/8700 spectrometer with the samples prepared as KBr pellets. UV–Vis absorption spectrum of the powder sample in the range of 200–1200 nm was recorded on a Varian Cary 5000 ultraviolet–visible (UV–Vis) near-infrared spectrophotometer. The powder XRD studies were carried out for doped and undoped materials on a PANalytical X'pert PRO diffractometer with Cu Kα radiation of wavelength $\lambda = 0.15406$ nm, 2θ values between 5° and 75°, at room temperature.

2.2. Preparation of single crystal of Mn(II) doped $[Zn(H_2O)_6][Zn(mal)_2(H_2O)_2]$

Solid zinc(II) basic carbonate is added to an aqueous solution of malonic acid under continuous stirring. The suspension is heated at 50–60 °C until a clear solution is obtained. This solution is filtered and mixed with an aqueous solution of the zinc(II) acetate. The solution is concentrated to 25 cm^3 in a steam bath and then it is allowed to grow single crystals doped with five different concentrations of manganese sulfate (0.1%, 0.5%, 1.0%, 2.0%, 5.0%) at room temperature. Well shaped, colorless single crystals suitable for EPR studies are obtained with in fifteen days.

3. Crystal structure

$[Zn(H_2O)_6][Zn(mal)_2(H_2O)_2]$ is isostuctural with $[Zn(H_2O)_6]$-$[Cu(mal)_2(H_2O)_2]$ (hereafter referred as HZBMC) [27]. HZBMC

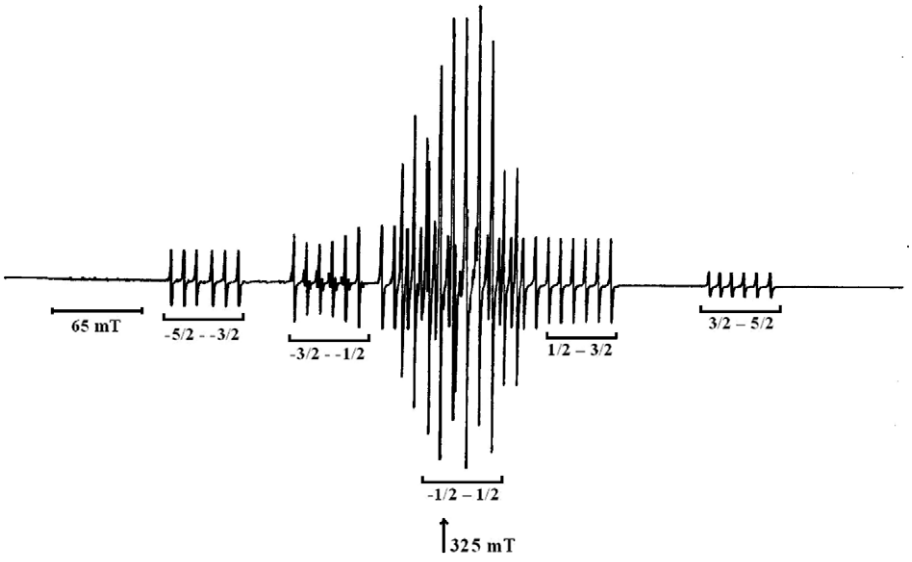

Fig. 1a. Single crystal EPR spectrum of Mn(II)/HZBMZ at room temperature when *B* is parallel to axis c^*. Frequency = 9. 34716 GHz.

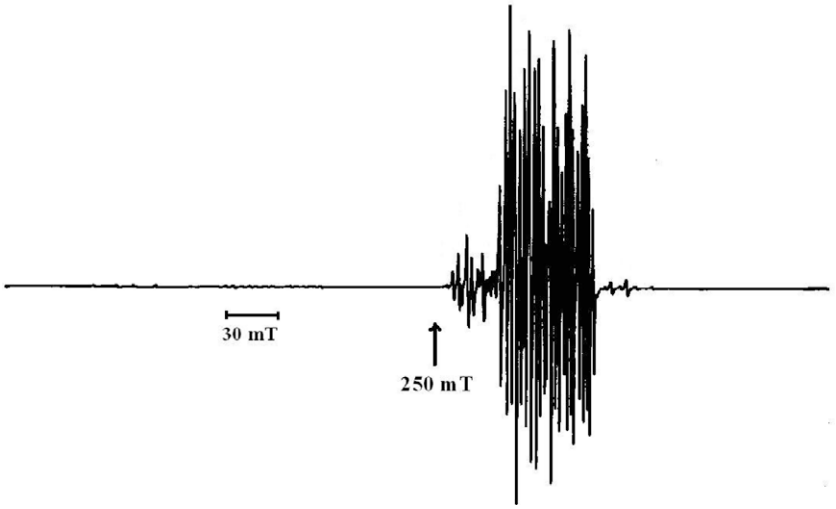

Fig. 1b. Single crystal EPR spectrum of Mn(II)/HZBMZ at room temperature when *B* is parallel to axis a^*. Frequency = 9. 32995 GHz.

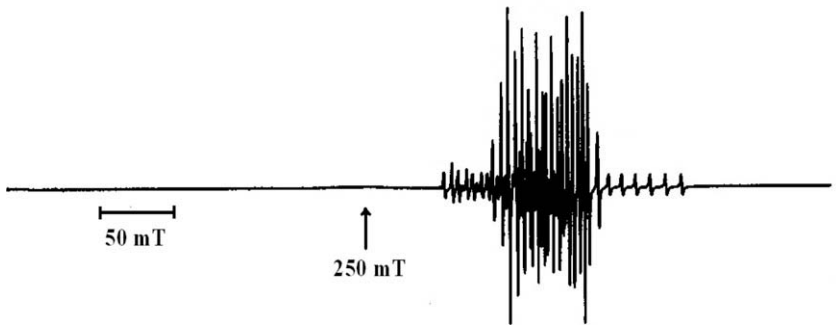

Fig. 1c. Single crystal EPR spectrum of Mn(II)/HZBMZ at room temperature when B is parallel to axis b. Frequency = 9. 34079 GHz.

belongs to triclinic crystal system with space group $P\bar{1}$, having unit cell parameters $a = 0.5274$ nm, $b = 0.7504$ nm, $c = 1.0314$ nm, $\alpha = 106.92°$, $\beta = 99.15°$, $\gamma = 95.81°$ and $Z = 2$. The coordination polyhedron of the copper atom in the anionic unit $[Cu(mal)_2(H_2O)]^{2-}$ is that of an elongated octahedral CuO_6. Four carboxylate oxygens from two bidentate malonate ligands build the equatorial plane, whereas two water molecules occupy the axial sites. The zinc(II) ion in the cationic units $[Zn(H_2O)]^{2+}$ is coordinated to six water molecules with a slightly distorted octahedral geometry.

4. Results and discussion

4.1. Single crystal EPR spectra

The ground state of Mn(II) ion, with a d^5 configuration is unique among d^n configurations, in that there is only one state with maximum spin multiplicity (^6S). This splits into three Kramers' doublets (±5/2, ±3/2 and ±1/2) in an orthorhombic crystalline field, which are further split in the presence of an applied magnetic field. These six levels give rise to five fine-structure transitions. Each fine-structure transition splits into six levels, due to nuclear spin of ^{55}Mn ($I = 5/2$) giving rise to 30 allowed transitions. However, in polycrystalline samples, only $|+1/2\rangle \leftrightarrow |-1/2\rangle$ transition is generally observed, since the other four transitions have large anisotropy [1]. If zero-filed splitting parameter (D) is very small compared to hyperfine coupling constant (A), the 30 line pattern will be so closely packed that one could see only six lines. On the other hand, if D is very large, one would expect five bunches of resonance lines, each splits into a sextet.

Single crystals of optimum size are selected for crystal rotations along the three mutually perpendicular crystallographic axes, i.e., a^*, b and c^*. Axis c^* is perpendicular to the crystal axis b in the bc crystal plane and axis a^* is orthogonal to b and c^*. In other words, a^*bc^* corresponds to orthogonal xyz coordinate system. As the crystals were grown with five different concentrations, crystals with 0.1 and 0.5 concentration show weak lines, where as crystals with 2.0% and 5.0% gave relatively broad lines. Hence, in all the further EPR measurements, crystals with concentration of 1.0% are used. However, 2.0% concentration samples are used for powder XRD measurements and 5.0% samples are employed for optical measurements. Single crystal EPR measurements of Mn(II)/HZBMZ at room temperature show a variety of complicated spectra. A typical EPR spectrum of Mn(II)/HZBMZ, when the applied magnetic field (B) is parallel to axis c^*, is shown in Fig. 1a. It clearly indicates a 30 line pattern. In addition, a few resonances are seen at the centre of the spectrum suggesting a second site, with relatively small zero-field value. This second site could not be followed during crystal rotations, due to its low intensity and overlap with the transitions of the other site. The transitions are marked in the figure. Another spectrum, when B is parallel to axis a^* is shown in Fig. 1b. Here, all the transitions are merged indicating a very low value of zero-field splitting (see below). Generally, one expects the intensity of fine-structure lines for Mn(II) system to be in the ratio of 5:8:9:8:5. However, in the present case, this ratio is randomly distributed in all the three planes. This may be due to the overlap other site, which shows at random orientations. Fig. 1c showing the single crystal EPR spectrum of Mn(II)/HZBMZ when the applied magnetic field (B) is parallel to axis b.

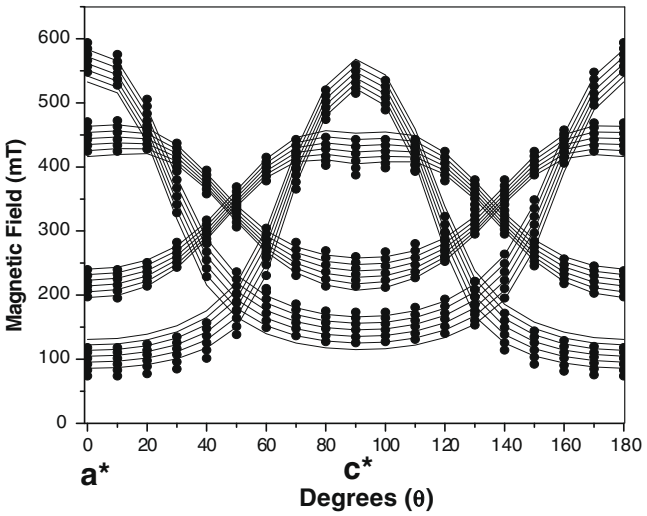

Fig. 2a. Iso-frequency plot of Mn(II)/HZBMZ for a^*c^* plane. Here $|\pm5/2\rangle \leftrightarrow |\pm3/2\rangle$ and $|\pm3/2\rangle \leftrightarrow |\pm1/2\rangle$ transitions only shown because $|+1/2\rangle \leftrightarrow |-1/2\rangle$ transition is difficult to follow. Solid circles indicate experimental values; solid lines correspond to theoretical values. $\nu = 9.34716$ GHz.

Crystal rotations are carried out in the three mutually orthogonal planes and iso-frequency plots in a^*c^* and bc^* planes are shown in Fig. 2a and b, respectively. In these figures, maximum spread is noticed at $\theta = 0°$ and the spread between two extreme fine-structures decreases as θ increases. At $\theta = 54.7°$, the fine-structure lines collapse. This orientation roughly corresponds to the magic angle, where D becomes zero. Further increase of θ, again increases the spread and the pattern is repeated. This shows that the angular variation of fine-structure follows a $(3\cos^2\theta - 1)$ variation. In the two iso-frequency plots, only the resonance lines corresponding to $(|\pm5/2\rangle \leftrightarrow |\pm3/2\rangle)$ and $(|\pm3/2\rangle \leftrightarrow |\pm1/2\rangle)$ are given, and resonance lines due to $|+1/2\rangle \leftrightarrow |-1/2\rangle$ transition, which are independent of D, are not given because of invariant. In Fig. 2a, it was noticed that the maxima in angular variation of $|5/2\rangle \leftrightarrow |3/2\rangle$ is shaper, whereas $|-5/2\rangle \leftrightarrow |-3/2\rangle$ is broad. A similar observation is noticed in Mn(II) doped malonato ligand complexes [28]. The reason is not yet known. From these iso-frequency plots, the spin-Hamiltonian parameters are calculated as mentioned below.

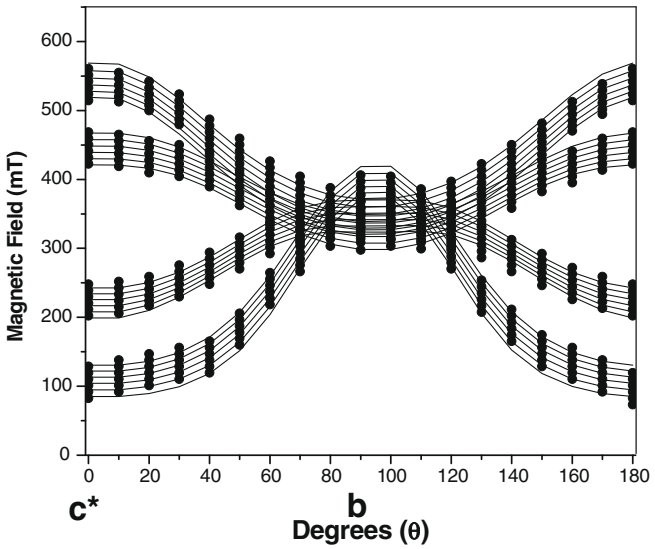

Fig. 2b. Isofrequancy plot of Mn(II) resonances in the bc^* plane of crystal lattice HZBMZ. Solid circles indicate experimental values, whereas solid lines correspond to theoretical values. ν = 9.34079 GHz.

4.2. Spin-Hamiltonian parameters

The spin-Hamiltonian for a spin sextet, including second order effects is given by [1]

$$H = \beta(g_{xx}B_xS_x + g_{yy}B_yS_y + g_{zz}B_zS_z) + (A_{xx}S_xI_x + A_{yy}S_yI_y + A_{zz}S_zI_z) + D\left[S_2^2 - \frac{1}{3}S(S+1)\right] + E\left(S_x^2 - S_y^2\right)$$

Here the first term represents the electron Zeeman interaction, the second represents the hyperfine interaction, the third term represents zero-field splitting and the fourth term represents deviation from axial symmetry. The spin-Hamiltonian parameters, obtained by using the resonance data in all the three planes with program EPR-NMR [29] are given in Table 1, along with the direction cosines. The direction cosines of metal–oxygen bonds have been calculated from the single crystal XRD data of the HZBMC and are given in Table 2. A few set of spin-Hamiltonian parameters, taken from literature are given in Table 3, for comparison, where a good agreement is noticed. As suggested earlier, deviation from axial symmetry is seen and the calculated E value is 15.6 mT.

Using the g and A values obtained in the EPR-NMR program, the iso-frequency plots are simulated for a^*c^* and bc^* planes and are also given in Fig. 2a and b. In these figures, solid lines correspond to theoretical variation and the solid circles correspond to the experimental data. A good agreement is observed in both the planes, confirming the accuracy of our calculated spin-Hamiltonian parameters (note the agreement in Fig. 2a at maxima).

Since the isotropic hyperfine coupling constant arises by the use of the polarization of the inner s-electrons, the sign of A for high spin Mn(II) complexes is always assigned as negative [30]. The sign of D is assigned relative to A by considering the separation between hyperfine lines at low field and high field. If the separation between hyperfine lines in the low field is greater than the high field, then the ratio D/A becomes positive or negative for the reverse case. In the present case, the separation increases from lower filed to higher field, D/A is negative. Since A is negative, D becomes

Table 2
The direction cosines of Zn–O bonds for HZBMC, obtained from the crystallographic data [27].

Zn–O bonds in HZBMC	Direction cosines		
	a^*	b	c^*
Zn–O (1w)	0.7389	−0.1537	−0.6559
Zn–O (2w)	−0.3862	0.6280	−0.6756
Zn–O (3w)	0.5328	0.7394	0.4117
Zn–O (1	0.6448	−0.7395	−0.1934
Zn–O (3)	−0.4591	−0.1025	−0.8825
Zn–O (4w)	0.0000	0.8275	−0.5614

Table 3
Spin-Hamiltonian parameters for Mn(II) in some related host lattices (D and A are in units of mT).

System	g	A	D	Ref.
MHMH[a]	1.997	−8.8	31.20	[31]
	2.013	−8.8		
	2.013	−8.8		
MMHH[b]	1.995	−9.6	33.44	[5]
	2.013	−10.6	32.17	
ZAPH[c]	2.002	−9.2	53.52	[32]
	2.001	−9.2	−35.41	
	2.001	−9.3	−18.11	
HZBMZ	1.972	−8.95	−34.49	Present work
	2.000	−9.48	−3.26	
	2.023	−9.93	37.74	
Powder values	1.994	9.07	46.23	

[a] MHMH – magnesium bis(hydrogen maleate) hexahydrate.
[b] MMHH – magnesium maleate hexahydrate.
[c] ZAPH – zinc ammonium phosphate hexahydrate.

Table 1
The spin-Hamiltonian parameters obtained from the single crystal rotations for Mn(II) doped in HZBMZ using the program EPR-NMR [29].

				Principal values	Direction cosines		
					a^*	b	c^*
g matrix							
	2.012	0.007	0.008	1.972	0.6028	0.1049	0.7909
		1.973	0.006	2.000	−0.7972	−0.1197	0.5917
			2.016	2.023	−0.0326	−0.9872	0.1558
A matrix (mT)							
	9.50	0.62	0.10	8.95	0.2366	0.0239	0.9713
		8.95	0.02	9.48	−0.9716	0.0109	0.2363
			9.90	9.93	−0.0049	−0.9996	0.0258
D matrix (mT)							
	37.68	−2.72	−2.16	−34.49	0.9995	0.0028	−0.0302
		−3.73	−3.79	−3.25	0.0065	−0.9925	0.1224
			−33.95	37.74	−0.0297	−0.1225	−0.9920

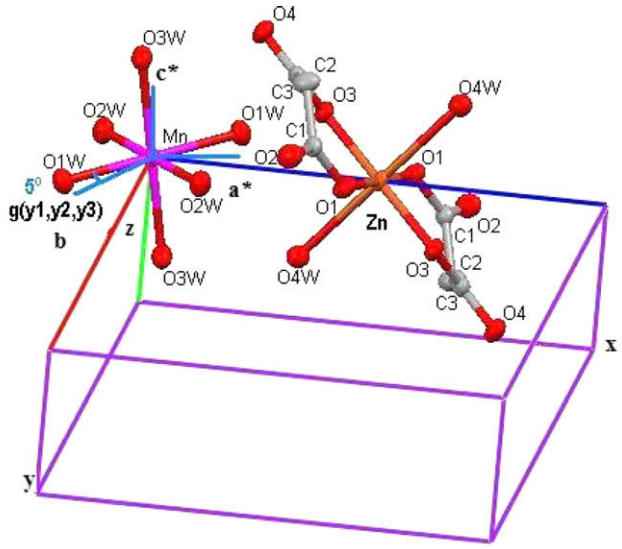

Fig. 3. Crystal structure of HZBMZ, assuming identical crystal structure of HZBMC [27], indicating the substitutional position of Mn(II) in HZBMZ and angle of deviation of Mn–O bond direction from *g* direction.

positive. This is also confirmed by measuring the spectra at lower temperature.

Generally, Mn(II) ions enter the lattice either substitutionally or interstitially. A survey of literature shows that Mn(II) ion invariably enters the Zn(II) host lattices substitutionally and this may be attributed to comparable ionic radii of Mn(II) (0.08 nm) and Zn(II) (0.08 nm). So it is reasonable, here also, to assume that the Mn(II) ions enter substitutionally at Zn(II) sites in the HZBMZ lattice.

4.3. Location of the impurity

The location of the impurity can be detected by comparing the direction cosines of the principal values of *g* and *A* tensors with any of the metal–ligand bond directions (Zn–O). The direction cosines of *g*, *A* and *D* are tabulated in Table 1 and that of metal–ligand bond direction cosine of HZBMC crystal lattice are given in Table 2. It is evident from the table that one of the direction cosines of the one of the principal *g*-values (2.0236) are found to match fairly well with that of the metal–oxygen (Zn–O1w) bond direction. The deviation between these directions is around 5°. This suggests that the Mn(II) ion has entered the lattice substitutionally and the location of *g* is shown in Fig. 3.

4.4. Polycrystalline EPR spectrum

In order to reconfirm the single crystal analysis, powder spectrum of the Mn(II)/HZBMZ is recorded at room temperature. The room temperature powder EPR spectrum is given in Fig. 4. Here one can notice clearly six lines (corresponding to $|+1/2\rangle \leftrightarrow |-1/2\rangle$ transition) indicating a single site of Mn(II) ion. Generally, due to large anisotropic effects in *D*, the other four transitions corresponding to ($|\pm5/2\rangle \leftrightarrow |\pm3/2\rangle$) and ($|\pm3/2\rangle \leftrightarrow |\pm1/2\rangle$) are weak. The powder spectrum is not symmetrical with respect to central portion of the spectrum indicating the presence of deviation from axial zero-field terms. This means that D_{xx} and D_{yy} are different. The powder EPR spectrum has been recorded at higher gain and modulation values to get the *D* value. Actually, the separation between second and fourth fine-structure lines is approximately equal to 4D, from which *D* has been estimated. The spin-Hamiltonian parameters (*g*, *A* and *D*) obtained from the powder spectrum, are also given in Table 3. These values agree well with the crystal data. Here, it is to be noted that *D* obtained from powder spectrum is related to D_{zz} by the equation, $D = (3/2)D_{zz}$ and $E = 1/2|(D_{xx} - D_{yy})|$.

4.5. Covalency of the metal–ligand bond

The percentage of covalency of the Mn–O bond has been calculated using Matamura's plot [33]. The covalency of the bond between manganese and its ligands depends on the isotropic hyperfine coupling constant *A*. The empirical relationship for the covalency of a bond between the *p* and *q* and their electronegativities χ_p and χ_q is given by

$$c = 1/n[1 - 0.16(\chi_p - \chi_q) - 0.035(\chi_p - \chi_q)^2]$$

Here, *n* is the number of ligands around Mn(II) ion. The percentage of covalency obtained from the above equation, assuming $\chi_{Mn} = 1.55$ and $\chi_O = 3.44$ is around 9.5%. The value of hyperfine splitting constant predicted from the graph (89.5×10^{-4} cm^{-1}) is in reasonable agreement with the observed value from powder spectrum.

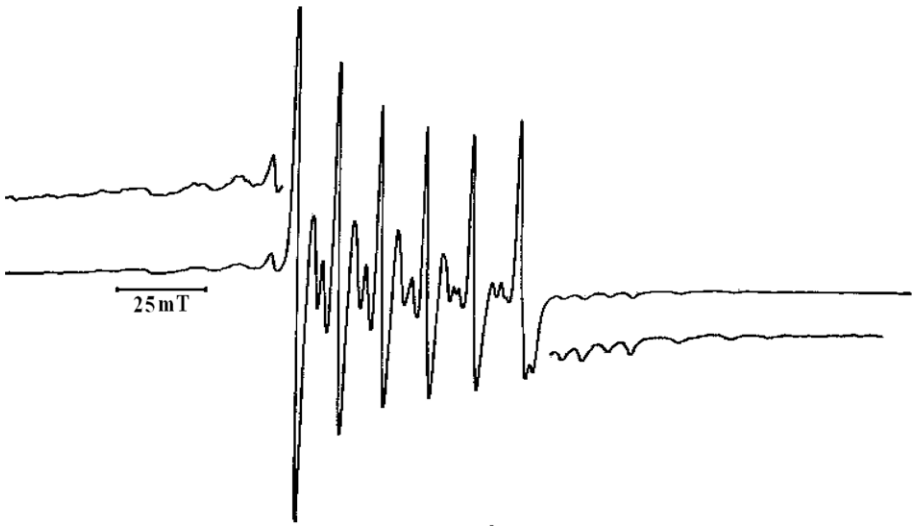

Fig. 4. Powder EPR spectrum of Mn(II) doped HZBMZ at room temperature. Frequency = 9.35505 GHz.

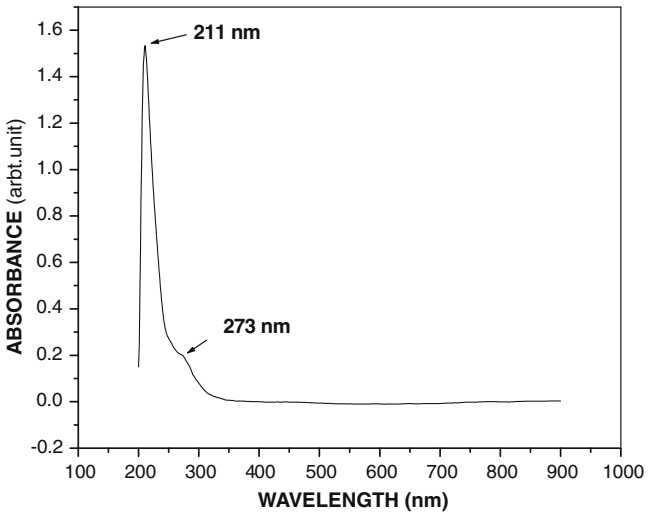

Fig. 5. Optical absorption spectrum of Mn(II) ion doped in HZBMZ at room temperature.

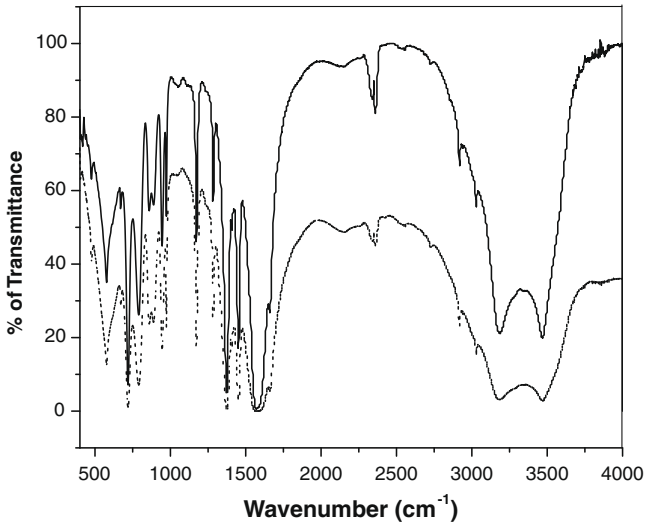

Fig. 6. FT-IR spectra of pure and Mn(II) ion doped HZBMZ at room temperature.

4.6. Optical absorption studies

Optical absorption spectrum of Mn(II) ion doped in HZBMZ, recorded at room temperature, is shown in Fig. 5. Mn(II) d–d absorption transitions are difficult to be seen as these are spin and parity forbidden in octahedral symmetry. However, charge transfer (CT) bands are parity allowed [34]. The sharp band at 211 nm is assigned to $^6A_{1g}(S) \rightarrow {}^4A_{2g}(F)$, the weak band at 273 nm is assigned to $^6A_{1g}(S) \rightarrow {}^4T_{2g}(D)$ of Mn(II) ion, which exits in the UV-region in absorption spectrum. The band at 273 nm is low in sharpness and intensity compared with 211 nm band. The strong and weak bands at 211 and 273 nm, respectively, have been attributed to the transitions of electron from ground state to excited states $^4A_{2g}(F)$, $^4T_{2g}(D)$, respectively.

4.7. FT-IR spectral studies

The infrared spectra of carboxylic acids display two important features: first due to very strong hydrogen bonding between the carboxyl groups of acid molecules, the bands will appear as strong and broad from 3400 to 2500 cm^{-1} stretching frequencies of the O–H single bond and second, the stretching frequency for the carbonyl group of the carboxylic acid appears in one of the two regions [35–37]. FT-IR spectra of HZBMZ and Mn(II) doped HZBMZ at room temperature are shown in Fig. 6. The infrared band positions and their tentative assignments for HZBMZ sample observed in the present work are given in Table 4.

Table 4
Observed FT-IR band positions and their tentative assignments for HZBMZ and Mn(II) ion doped HZBMZ.

Band positions (cm^{-1})		Assignments
HZBMZ	Mn doped HZBMZ	
719	719	Zn–O
791	793	Zn–O + O–C–O
860, 945	862, 945	Zn–O–H
1170, 1280	1170, 1280	–C–H
1370, 1386	1370, 1386	
1428, 1408	1428, 1408	–O–H (bending)
1654	1654	(C=O) + (C–H)
1570, 2340	1570, 2340	H–O–H
2920	2920	$–CH_2–$
3030, 3190	3030, 3190	$–OH_2$
3470	3470	–OH

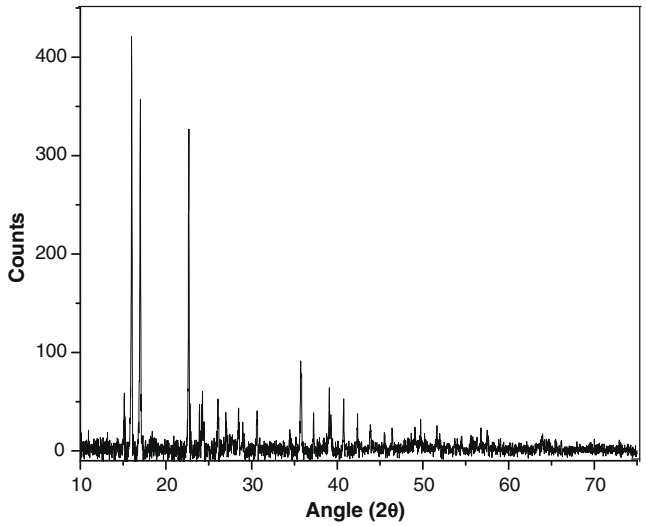

Fig. 7. Powder XRD pattern of Mn(II) doped HZBMZ at room temperature.

Table 5
The calculated lattice parameters of HZBMZ and Mn(II) doped HZBMZ from powder XRD, along with single crystal XRD of HZBMC [27].

Lattice parameters (nm) of HZBMC from single crystal XRD	Lattice parameters (nm) calculated from powder XRD	
	HZBMZ	Mn doped HZBMZ
$a = 0.5274$	$a = 0.5382$	$a = 0.5382$
$b = 0.7504$	$b = 0.7424$	$b = 0.7424$
$c = 1.0314$	$c = 1.1293$	$c = 1.1293$

4.8. Powder XRD studies

Powder XRD pattern of Mn(II) doped HZBMZ at room temperature is shown in Fig. 7. According to powder XRD measurements, Mn(II) doped HZBMZ powder sample has identical lattice parameters as HZBMZ powder sample, as expected from the low impurity

concentration. The lattice parameters are tabulated in Table 5 with the single crystal XRD parameter of HZBMC [27]. It is clear from the table that the parameters of HZBMZ and Mn(II) doped HZBMZ matched with reported values of copper complex [27], confirming that the zinc complex is isomorphic with copper complex and the low dopant concentration of Mn(II) in HZBMZ does not alter the symmetry of host lattice.

5. Conclusion

EPR spectra of Mn(II) doped HZBMZ have been studied at room temperature. The angular variation reveals the presence of more than one site, which correspond to distinct sites of Mn(II). The detailed EPR analysis of one site indicates that Mn(II) ion has entered the lattice substitutionally. The evaluated spin-Hamiltonian parameters reflect orthorhombic symmetry. The magnitude of the hyperfine splitting constant *A* indicates that the bonding between the paramagnetic ion and the ligand is ionic in nature. The large *D* and *E* values reveal the distortion present in the crystal lattice due to steric effects of the crystal packing caused by malonate ligands. From the observed band positions assigned to charge transfer transition in the UV-region, the Mn(II) ions are in a distorted octahedral symmetry. The observed bands in the FT-IR spectrum have been assigned to Zn–O, O–H, –C=O, –C–O, $–CH_2–$ and H_2O bonds. Powder XRD confirms the formation of HZBMZ which is isomorphous with HZBMC.

Acknowledgments

P.S.R. and S.B. thank CSIR, New Delhi for providing financial assistance. P.S.R. also thanks DST and UGC for financial assistance.

References

[1] A. Abragam, B. Bleaney, Electron Paramagnetic Resonance of Transition Ions, Clarendon Press, Oxford, 1970.
[2] V.S.X. Anthonisamy, M. Velayutham, R. Murugesan, Physica B 262 (1999) 13.
[3] V.K. Jain, V. Kapoor, V. Prakash, Solid State Commun. 97 (1996) 425.
[4] P. Sambasiva Rao, Spectrochim. Acta A 49 (1993) 897.
[5] Jessiamma Joseph, P. Sambasiva Rao, Spectrochim. Acta A 52 (1996) 607.
[6] P. Sambasiva Rao, S. Subramanian, Mol. Phys. 54 (1985) 429.
[7] D.J. Attanasio, J. Magn. Reson. 26 (1977) 81.
[8] R. Murugesan, A. Thamaraichelvan, A.M. Franklin, V. Ramakrishnan, Mol. Phys. 79 (1993) 663.
[9] G.C. Upreti, R.S. Saraswat, Magn. Reson. Rev. 7 (1982) 215.
[10] G.C. Upreti, J. Magn. Reson. 14 (1974) 247.
[11] Wen-Chen Zheng, Phys. Status Solidi B 205 (1998) 627.
[12] S.N. Rao, Y.P. Reddy, P.S. Rao, Solid State Commun. 82 (1992) 419.
[13] R. Murugesan, V.S.X. Anthonisamy, S. Subramanian, Spectrochim. Acta A 49 (1993) 1801.
[14] C. Ruiz-Perez, Y. Rodriguez-Martin, M. Hernandez-Molina, F.S. Delgado, J. Pasan, J. Sanchiz, F. Lloret, M. Julve, Polyhedron 22 (2003) 2111.
[15] J. Pasan, F.S. Delgado, Y. Rodriguez-Martin, M. Hernandez-Molina, C. Ruiz-Perez, J. Sanchiz, F. Lloret, M. Julve, Polyhedron 22 (2003) 2143.
[16] C. Oldham, in: G. Wilkinson, R.D. Gillard, J.A. McCleverty (Eds.), Comprehensive Coordination Chemistry, vol. 2, Pergamon Press, Oxford, 1987, p. 435.
[17] D.K. Towle, S.K. Hoffmann, W.E. Hatfield, P. Singh, P. Chaudhuri, Inorg. Chem. 27 (1988) 394.
[18] P.R. Levstein, R. Calvo, Inorg. Chem. 29 (1990) 1581.
[19] F. Sapiña, E. Escrivá, J.V. Folgado, A. Beltrán, A. Fuertes, M. Drillon, Inorg. Chem. 31 (1992) 3851.
[20] E. Colacio, J.P. Costes, R. Kivekäs, J.P. Laurent, J. Ruiz, Inorg. Chem. 29 (1990) 4240.
[21] E. Colacio, J.M. Domínguez-Vera, J.P. Costes, R. Kivekäs, J.P. Laurent, J. Ruiz, M. Sundberg, Inorg. Chem. 31 (1992) 774.
[22] E. Ruiz, Inorg. Chem. 212 (1993) 115.
[23] A.N. Papadopoulos, Inorg. Chem. 35 (1996) 559.
[24] V. Tangoulis, D.A. Malamatari, K. Soulti, V. Stergiou, C.P. Raptopoulos, A. Terzis, T.A. Kabanos, D.P. Kessissoglou, Inorg. Chem. 35 (1996) 4974.
[25] H. Li, C.E. Davis, T.L. Groy, D.G. Kelley, O.M. Yaghi, J. Am. Chem. Soc. 120 (1998) 2186.
[26] S.K. Chawla, A. Arora, K. Nattinen, K. Rissanen, J.V. Yakhmi, Polyhedron 23 (2004) 3007.
[27] Y. Rodriguer-Martin, J. Sanchiz, C. Ruiz-Perez, F. Lloret, M. Julve, Cryst. Eng. Commun. 4 (2002) 631.
[28] B. Natarajan, Ph.D. Thesis, Submitted to Pondicherry University, Pondicherry, 2007.
[29] EPR-NMR Program developed by F. Clark, R.S. Dickson, D.B. Fulton, J. Isoya, A. Lent, D.G. McGavin, M.J. Mombourquette, R.H.D. Nuttall, P.S. Rao, H. Rinnerberg, W.C. Tennant, J.A. Weil, University of Saskatchewan, Saskatoon, Canada, 1996.
[30] M. Korkman, M. Dupont, B. Aktas, J. Phys. Chem. Solids 45 (1984) 465.
[31] R.M. Krishna, V.P. Seth, R.S. Bensal, I. Chand, S.K. Gupta, J.J. Andre, Spectrochim. Acta A 54 (1998) 517.
[32] P. Chand, O.P. Agarwal, Spectrochim. Acta A 47 (1991) 775.
[33] O. Matumura, J. Phys. Soc. Jpn 14 (1959) 108.
[34] R. Selomulya, S. Ski, K. Pita, C.H. Kam, Y. Zhang, S. Buddhudu, Mater. Sci. Eng. B 100 (2003) 136–141.
[35] K. Nakamoto, Infrared and Raman Spectra of Inorganic and Coordination Compounds, 4th ed., John Wiley Interscience, New York, 1986. p. 231.
[36] N.O. Gopal, K.V. Narasimhulu, Lakshmana Rao, J. Phys. Chem. Solids 63 (2002) 295.
[37] R.M. Silerstein, G. Clayton Bassler, T.C. Morril, Spectrometric Identification of Organic Compounds, 5th ed., Wiley, New York, 1991.